International Journal of Smart Grid and Clean Energy

Apply blade element momentum theory in matching a wind turbine system

Jui –Hsiang Kao, Yan-Jhang Lin, Yu-Why Huang

Department of Systems Engineering and Naval Architecture National Taiwan Ocean University No.2, Peining Rd., Jhongjheng District, Keelung City 20224, Taiwan

Abstract

The objective of this paper is to apply Blade Element Momentum Theory in matching the turbine blades and the generator to increase the efficiency of the wind turbine, and the matching process is developed. As the turbine blades are not matched well with the generator in advance, the optimal design of the turbine blades can't attain the expected performance, and the controller can't increase the power capture. Thus, the matching problem is worthy of being discussed. The T (torque)–N (r/min) curves of turbine blades are calculated by Blade Element Momentum Theory. As the optimal voltage mode of the generator is selected, the characteristics of the operating points, such as tip speed ratio, revolutions per minute, blade torque, and efficiency, can be identified by the crossover point of the T–N curves of the turbine blades and the generator. A horizontal upwind turbine is treated as the study case here to illustrate the computing and matching processes.

Keywords: Blade element momentum theory, turbine blades, generator, T–N curve, tip speed ratio

1. Introduction

In order to gain the maximum power from the turbine system, the research method adopted generally centers on the hydrodynamic simulation of turbine blades and the logic setting of the controller; matching the two systems, the turbine blades and the generator, is relatively rare. In a poorly-matched turbine system, the caused breakdown in efficiency is usually more than 15%. Therefore, this study utilizes Blade Element Momentum Theory to match the two systems, and the matching process will be developed.

Traditionally the turbine blades were design by BEM (Blade element momentum) as discussed in Glauert (1963) [1]. Dynamic stall corrections were adopted by Leishman (1989) [2] to improve BEM theory. However, the interaction of rotational flow and 3D blades cannot be described clearly by BEM. Hirsch (1990) [3] applied CFD in blade simulation. According to Bardina et al. (1997) [4], it was commented that the SST k-ω turbulence model derived by the Menter (1994) [5] is suitable for predicting the flows with separation under adverse pressure gradients. Fingersh et al. (2001) [6], and Hand et al. (2001) [7] conducted the aerodynamic experiments of turbine blades in wind tunnel and provided valuable test data for 3-D CFD Rotor analyses. In Mukesh et al. (2013) [8], a case study in which the capability of CFD in predicting complex 3D wind turbine aerodynamics is demonstrated with NREL Phase VI data. Reasonably good agreement is obtained when comparing modeled mechanical effects Viz. power, thrust, and span wise force components with measurements over wind speeds ranging from 5m/s to 25m/s. Imamura (2003) [9] indicated Blade Element Momentum Theory is an effective method to analysis the horizontal axis wind turbine (HAWT). Blade Element Momentum Theory is derived by combining angular momentum theory and Blade Element Theory. The interference of wind turbine surge motion was discussed in Tran and Kim (2016) [10] by CFD and Blade Element Momentum Theory, and

* Manuscript received October 20, 2018; revised November 1, 2019.
Corresponding author. Tel+49 (0) 75717329250; *E-mail address*: mast@hs-albsig.de
doi: 10.12720/sgce.9.1.44-51

the result indicated that the unsteady aerodynamic thrust and power tend to vary considerably depending on the oscillation frequency and amplitude of the surge motion. Eftichios and Kostas (2006) [11] applied the Perturb and Observe Algorithm to track the maximum power of the turbine system by the controller. Experimental results of the proposed system indicated near-optimal generator output power, increased by 11%-50% compared to a generator directly connected via a rectifier to the battery bank. Adam et al. (2007) [12] set Fuzzy Logic in the controller to gain the maximum power. According to Odgaard et al. (2016) [13], multi-objective MPC (Model predictive control) problems are tuned by using Pareto curves to minimize cost of energy of the wind turbine system. The evaluation showed a good potential of using MPC.

In this paper, Blade Element Momentum Theory is applied to match the turbine blades and the generator for gaining the optimal operating point. A horizontal upwind turbine is analyzed by Blade Element Momentum Theory; then, matched with the selected generator. Both matched and unmatched results will be compared to evidence the improvement of the final efficiency.

2. Blade Element Momentum Theory

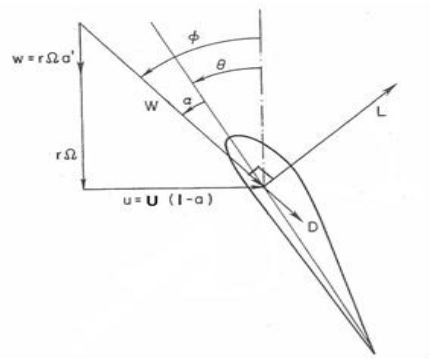

Fig. 1. Inflow analysis of the blade section

The detail of the derivations for Blade Element Momentum Theory could be referred in Tony et al. (2001) [14]. This section will organize the key equations which will be applied in analyzing turbine blades. Fig. 1 indicates the inflows of the blade section. U and U(1-*a*) are the axial velocities for far upstream and blade rotating plane respectively, where a is the axial induction factor. The tangential velocity of the fluid due to the acceleration round an airfoil is r$\Omega a'$, and the rotating speed is rΩ, where *a'* is the tangential component of the induced flow, and r is the radial dis-tance of the blade section. The tangential inflow is rΩ(1+*a'*). Thus the geometrical attack angle, Φ, could be given by the following expression:

$$\tan\phi = \frac{U(1-a)}{\Omega r(1+a)} \tag{1}$$

In Fig. 1, the relation between the section pitch angle, θ, and inflow attack angle, α, is as below.

$$\alpha = \phi - \theta \tag{2}$$

Both *a* and *a'* are defined with the resulting lift and drag coefficients of the airfoil:

$$a = 1 - \frac{1}{\frac{\sigma_r}{4\sin^2\phi}\left(C_l\cos\phi + C_d\sin\phi\right)+1} \tag{3}$$

$$a' = \frac{1}{1-\frac{\sigma_r}{4\sin\phi\cdot\cos\phi}\left(C_l\sin\phi - C_d\cos\phi\right)} - 1 \tag{4}$$

C_l, and C_d are the coefficients of lift and drag for the airfoil respectively. σ_r is the local solidity of the rotor:

$$\sigma_r = \frac{N_B \cdot c}{2\pi r} \tag{5}$$

c is the chord length of the foil, and NB is the number of blade number.

According to Blade Element Theory [14], the blade efficiency, C_p, can be represented by Equation (6).

$$C_P = \frac{8}{\lambda_{tip}^2}\int_{\lambda_{hub}}^{\lambda_{tip}} \lambda_r^3 a'(1-a)\left(1-\frac{C_d}{C_l}\cos\phi\right)d\lambda_r = \frac{8}{\lambda_{tip}^2}\sum_{i=hub}^{i=tip}\lambda_i^3 a_i'(1-a_i)\left(1-\frac{C_d}{C_l}\cos\phi_i\right)\Delta\lambda \tag{6}$$

$$\lambda_r = \frac{2\pi n r}{V} \tag{7}$$

The integration shown in Equation (6) is from blade hub to blade tip. λ_r is the local tip speed ratio, n the rotor speed, and V is the wind speed.

In this paper, the geometry of the turbine blade is known, and performance of the turbine blade (C_P ~ λ_{tip} curve) should be predicted by Blade Element Momentum Theory. Then, the predicted results will be imposed to match the generator for attaining high efficiency. Following is the flow chart (Fig. 2) of the proposed scheme for each blade section (i.e. each foil at different radial position). In Fig. 2, a iterating scheme is carried out to get convergent values of a and a', iterations for a constant rotating speed are conducted in a loop. As a and a' are obtained, the blade efficiency in the constant rotating speed can be determined by Equation (6). In each loop, the rotating speed a given a specified value. Therefore, the complete C_P ~ λ_{tip} curve can be found after several loops.

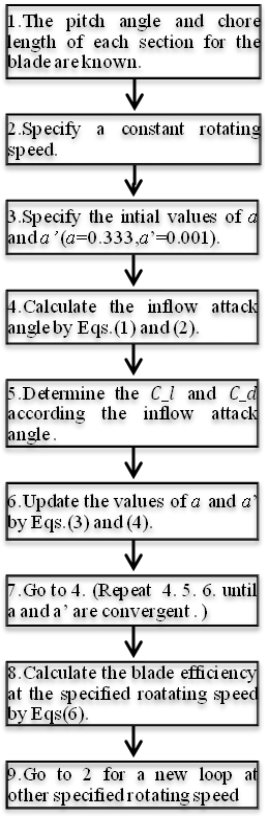

Fig. 2. The flow chart of the iterating scheme

Fig. 3. The outline of the discussed wind turbine

3. Analysis of Turbine Blades

Table 1. The geometrical parameters of the discussed wind turbine

Rotor Radius (R) in meter	Number of Blades	Foil Type of Blades
1.85	3	NACA-4415
r/R	Pitch angle θ (deg)	Chord length (m)
0.3	14.2	0.29
0.4	10.04	0.24
0.5	7.21	0.2
0.6	5.19	0.17
0.7	3.69	0.14
0.8	2.54	0.13
0.9	1.62	0.11
0.95	1.24	0.11

In this paper, a horizontal upwind turbine shown in Fig. 3 is taken as the computing sample. The geometrical parameters of the discussed wind turbine are known and listed in Table 1. The values of C_l, and C_d for the selected section, NACA-4415 at different inflow attack angle, α, is plotted in Fig. 4. A Fortran code is developed according the flow chart shown in Fig. 2. The $C_P \sim \lambda_{tip}$ curve obtained by the developed code is shown in Fig. 5. C_p is the blade efficiency; it is a function of the blade torque (T) and the rotating speed (N).

$$C_p = \frac{2 \cdot \pi \cdot N \cdot T}{1/2 \cdot \rho \cdot V^3 \cdot A} \tag{8}$$

Fig. 5 shows that when the TSR of the operating point for this wind turbine is located at 4.3~7.1, the blades will operate more efficiently. According to Fig. 5, and Equation (8), the T (torque)-N (RPM) curves of the turbine blades at different wind speeds can be plotted as Fig. 6.

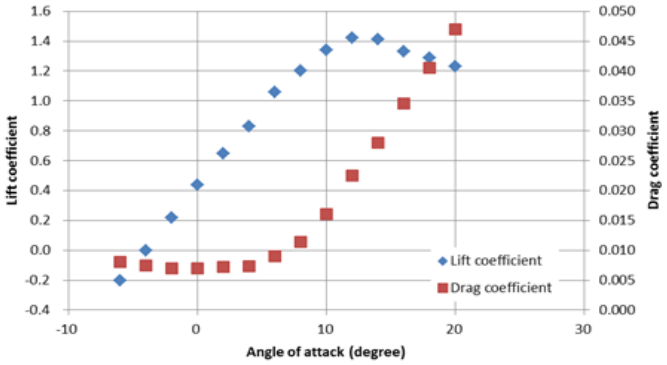

Fig. 4. Drag and lift coefficients at different attack angle for NACA-4415

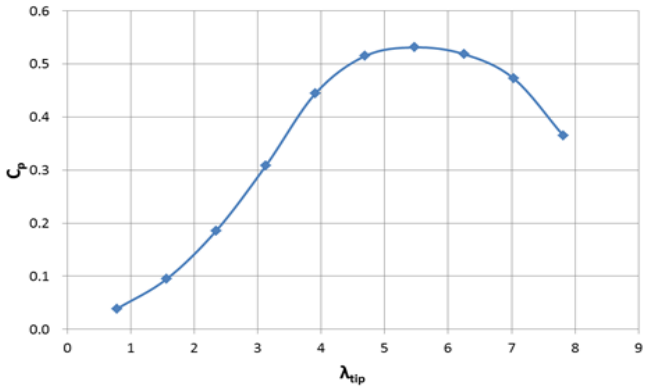

Fig. 5. The CP ~λtip curve of the turbine blades

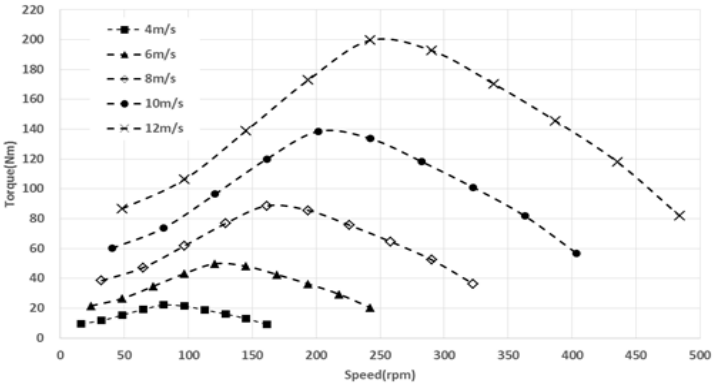

Fig. 6. The T (torque)-N (RPM) curves at different wind speeds

4. Matching the Turbine Blades with the Generator

The selected generator, to be matched with the turbine blades, is a direct-drive type with a 3-phase permanent NdFeB magnet. The measured T-N curves of this generator with every CV (constant-voltage output) model are plotted in Fig. 7 and the corresponding efficiencies are shown in Fig. 8. According to Fig. 8, for any CV mode the maximal efficiency is larger than 80%; the slope varies rapidly before reaching the maximal efficiency point. It is in this steep-slope region, that the breakdown in efficiency happens. For attaining high efficiency, the location of the operating point should not be in the steep-slope region

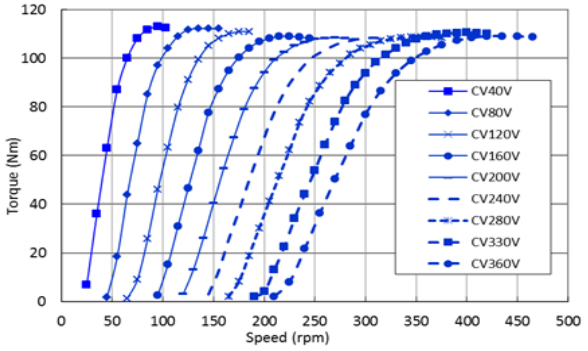

Fig. 7. The T-N curves of this generator tested by CV model

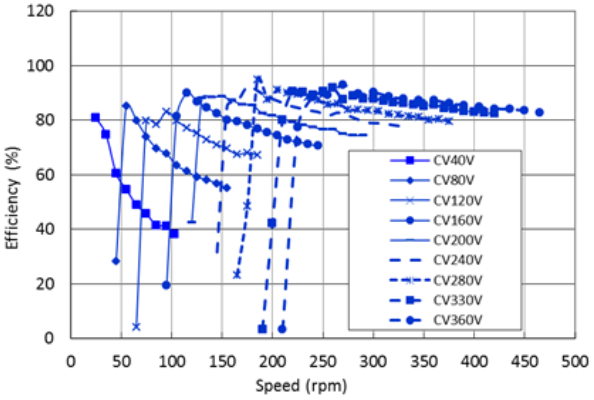

Fig. 8. The efficiency of this generator

For a wind turbine system, the torque generated by the blades is used to overcome the torque of the generator. In this way, the mechanical energy can be transferred to electronic energy by the generator. Thus the data shown in Figs. 6 should be matched with those shown in Fig. 7. Fig. 9 is obtained by combining Figs. 6 and 7. From Fig. 9, the operating point (i.e. the matched point) at every wind speed can be determined. At the optimal operating point, both the efficiencies of turbine blades and the generator should be kept high. The efficiency of the turbine blades varies with the tip speed ratio, as shown in Equation (7), λ_{tip}. As shown in Fig. 5, when the λ_{tip} of the operating point for this wind turbine is located at 4.3~7.1, the blades will become more efficient. Besides, it should be noted that the operating speed, RPM, cannot be in the steep-slope region of the selected CV mode, as shown in Fig. 8. In this steep-slope region, the efficiency of the generator will obviously be reduced. Thus, the criteria for the choice of operating points are the λ_{tip}-C_p curve as shown in Fig. 5, the efficiency curves of the generator at every CV mode as shown in Fig. 8, the determined operating speed, RPM, and the selected CV mode of the generator. It is expected that the TSR value calculated by the determined RPM will be located in the high-efficiency region of Fig. 5, and not in the steep-slope region of the selected CV mode in Fig. 8.

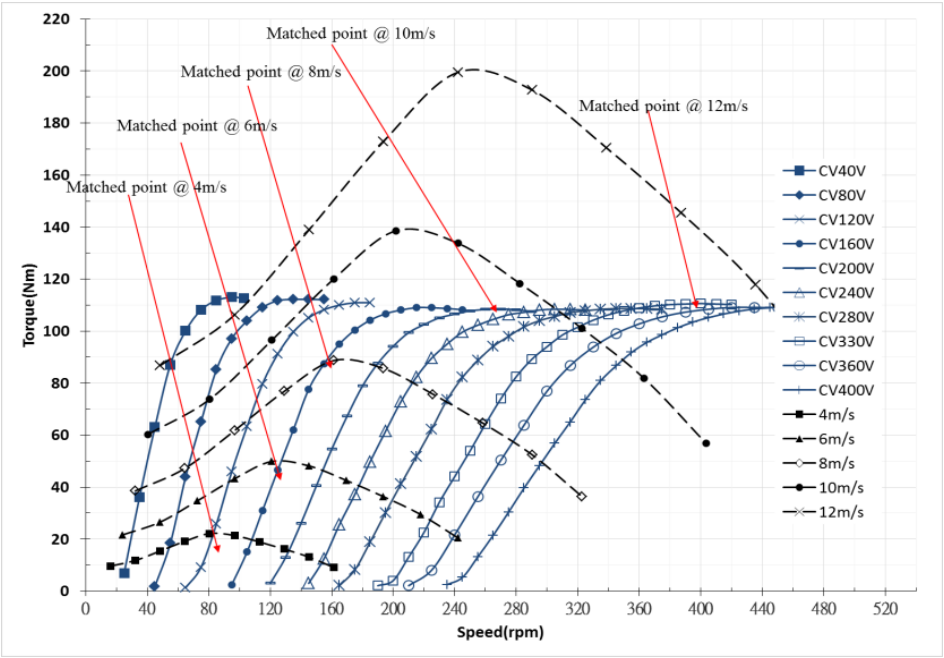

Fig. 9. The efficiency of this generator

Table 2. The unmatched operating points at every wind speed

V(m/s)	RPM	CV	eff-g	eff-e	Cp	P-blade	P-out	TSR
4	108	160	0.84	0.9	0.54	238.1	179.9	5.2
6	154	200	0.88	0.9	0.53	789.3	625.7	5
8	189	200	0.83	0.9	0.51	1801.9	1341.2	4.6
10	306	240	0.79	0.9	0.53	3659.4	2596.7	5.9
12	449	400	0.86	0.9	0.45	5394.3	4161.9	7.2

Table 2 shows the associated information of each matched operating point for every wind speed. Take 6m/s wind speed for example. A CV 200V mode of generator is selected as the electronic control model. According to Fig. 9, the matched point of 6m/s corresponds to 154RPM and 48 Nm. From Fig. 8 we can see that the generator efficiency, eff_{-g}, of CV 200V at 154RPM is 88%. The electronic efficiency, eff_{-e}, is usually 90~93%, and is assumed to be 90% here. The blade efficiency is about 53% as calculated by Equation (8). P_{-blade} (i.e. the mechanical power), 789W, and P_{-out} (i.e. the final electronic power), 625W, are computed by the following:

$$P_{-blade} = 2 \cdot \pi \cdot N \cdot T \tag{9}$$

$$P_{-out} = P_{-blade} \cdot eff_{-g} \cdot eff_{-e} \tag{10}$$

According to Fig. 5, when the TSR value of the operating point is in the range 4.3~7.1, the blades will achieve greater efficiency. Besides, the matched speed, 154RPM, is not found in the steep-slope region shown in Fig. 8; the generator efficiency, eff_{-g}, is also kept high.

5. Conclusions

The main purpose of this paper was to develop a matching process for turbine blades and generator to improve the efficiency of the wind turbine system. At different CV model, the T (torque)-N (RPM) curves of the generator are measured. The T (torque)-N (RPM) curves of turbine blades are iterated according to Blade Element Momentum Theory. Both the T (torque)-N (RPM) curves of the turbine blades and the generator are plotted together to find the optimal operating points. The basis for choosing the operating points are: the selected CV mode of the generator, the TSR-Cp curve of the turbine blades, the efficiency curves of the generator at every CV mode, and the determined operating speed, RPM. It is suggested that the determined RPM be located in the high-efficiency region of the TSR-Cp curve of the turbine blades, not in the steep-slope region of selected CV mode. The proposed method of achieving an optimal balance of turbine and generator is still in the developmental stage. Over-speed protection and noise abatement during the matching process are areas that warrant future discussion. The expectation should be that the matched rotating speed is under control as the wind turbine experiences gusts, and does not cause unacceptable noise. The above concerns are suggested for future study to make this present process robust.

Conflict Interest

This paper was not carried out with a conflict of interest.

Author Contributions

Jui –Hsiang Kao programed the code, and wrote the paper. Yan-Jhang Lin helped to analyze the data. Yu-Why Huang plotted the figures according to the calculated results.

References

[1] Glauert H. *Airplane Propellers, in Aerodynamic Theory*. W. F. Durand, Ed., Dover, New York, USA; 1963.

[2] Leishman JG. A semi-empirical model for dynamic stall. *Journal of the American Helicopter Society*, 1989; 34(3): 3-17.

[3] Hirsch C. *Numerical Computation of Internal and External Flows*. Wiley; 1990.

[4] Bardina JE, Huang PG, Coakley TJ. *Turbulence Modeling Validation, Testing, and Development*. NASA Technical Memorandum No. 110446, 1997.

[5] Menter FR. Two-equation eddy-viscosity turbulence models for engineering applications. *AIAA J.*, 1994; 32(8): 1598-1605.

[6] Fingersh LJ, Simms D, Hand M, Jager D, Contrell J, Robinson M, Schreck S, Larwood S. Wind tunnel testing of NREL's unsteady aerodynamics experiment. *AIAA–2001-0035*, *ASME Wind Energy Symposium*, Reno, NV, 2001.

[7] Hand MM, Simms DA, Fingersh LJ, Jager DW, Cotrell JR, Schreck S, Larwood SM. Unsteady aerodynamics experiment phase VI: Wind tunnel test configurations and available data campaigns. National Renewable Energy Laboratory, NREL/TP-500e29955, 2001.

[8] Mukesh M, Yelmule, Eswara Rao Anjuri VSJ. CFD Predictions of NREL Phase VI Rotor Experiments in NASA/AMES Wind Tunnel. *International Journal of Renewable Energy Research*, 2013; 3(2).

[9] Imamura H. Aerodynamics of wind turbines. *Joint Action Symposiums on Aerodynamics for Wind Turbines*, Colorado, U. S. A., 2003.

[10] Tran TT, Kim DH. 2016. A CFD Study into the influence of unsteady aerodynamic interference on wind turbine surge motion. *Renewable Energy*, 2016; 90: 204-228.

[11] Eftichios K, Kostas K. Design of a maximum power tracking system for wind-energy-conversion applications. *IEEE Transactions on Industrial Electronics*, 2006; 53(2): 486-494.

[12] Adam M, Xavier R, Frederic R. Architecture complexity and energy efficiency of small wind turbines. *IEEE Transactions on Industrial Electronics*, 2007; 54(1).

[13] Odgaard PF, Larsen LFS, Wisniewski R, Hovgaard TG. On using Pareto optimality to tune a linear model predictive controller for wind turbines. *Renewable Energy*, 2016; 87(2): 884-891.

[14] Tony B, David S, Nick J, Ervin B. *Wind Energy Handbook*. John Wiley & Sons, LTD; 2001.